ACS chemical biology

Articles

pubs.acs.org/acschemicalbiology

Bile Acid Recognition by NAPE-PLD

Eleonora Margheritis,[†] Beatrice Castellani,[‡] Paola Magotti,[‡,#] Sara Peruzzi,[†] Elisa Romeo,[‡] Francesca Natali,[§] Serena Mostarda,[∥] Antimo Gioiello,[∥] Daniele Piomelli,[‡,⊥] and Gianpiero Garau*[,†,‡]

[†]Center for Nanotechnology Innovation@NEST, Istituto Italiano di Tecnologia, Piazza San Silvestro 12, 56127 Pisa, Italy

[‡]Department of Drug Discovery-Validation, Istituto Italiano di Tecnologia, Via Morego 30, 16163 Genoa, Italy

[§]Institute Laue-Langevin (ILL) and CNR-IOM, 71 avenue des Martyrs, 38042 Grenoble, France

[∥]Department of Pharmaceutical Sciences, University of Perugia, Via del Liceo 1, 06125 Perugia, Italy

[⊥]Department of Anatomy & Neurobiology, University of California - Irvine, Gillespie NRF 3101, Irvine, California 92697, United States

ABSTRACT: The membrane-associated enzyme NAPE-PLD (N-acyl phosphatidylethanolamine specific-phospholipase D) generates the endogenous cannabinoid arachidonylethanolamide and other lipid signaling amides, including oleoylethanolamide and palmitoylethanolamide. These bioactive molecules play important roles in several physiological pathways including stress and pain response, appetite, and lifespan. Recently, we reported the crystal structure of human NAPE-PLD and discovered specific binding sites for the bile acid deoxycholic acid. In this study, we demonstrate that in the presence of this secondary bile acid, the stiffness of the protein measured by elastic neutron scattering increases, and NAPE-PLD is ∼7 times faster to catalyze the hydrolysis of the more unsaturated substrate N-arachidonyl-phosphatidylethanolamine, compared with N-palmitoyl-phosphatidylethanolamine. Chenodeoxycholic acid and glyco- or tauro-dihydroxy conjugates can also bind to NAPE-PLD and drive its activation. The only natural monohydroxy bile acid, lithocholic acid, shows an affinity of ∼20 μM and acts instead as a reversible inhibitor ($IC_{50} \approx 68$ μM). Overall, these findings provide important insights into the allosteric regulation of the enzyme mediated by bile acid cofactors and reveal that NAPE-PLD responds primarily to the number and position of their hydroxyl groups.

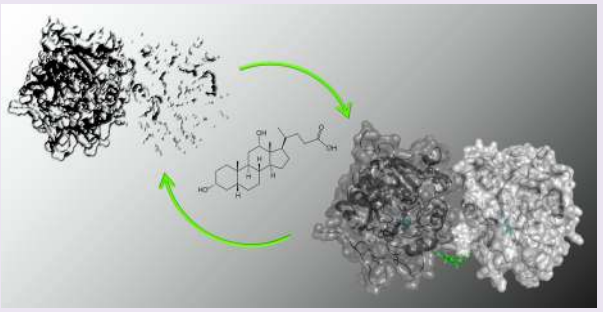

Lipid signaling molecules and their enzymes constitute a complex network with multiple nodes of interaction and cross-regulation.[1] Deciphering these nodes can provide essential clues to their signaling mechanisms. Among bioactive lipidic molecules, the amides of fatty acids with ethanolamine (FAE) promote essential neurological, cyto-protective, and metabolic actions. The endogenous cannabinoid arachidonylethanolamide (anandamide) is known to elicit analgesic and anxiolytic actions in rodents by activating cannabinoid receptors in central and peripheral neurons.[2] Anandamide contributes to stimulating appetite,[3−7] addiction,[8] and brain synaptogenesis.[9] Oleylethanolamide is another important lipid amide that regulates body weight and lifespan, engaging nuclear peroxisome proliferator-activated receptors.[10−12] Palmitoylethanolamide serves as an early stop signal that contrasts the progress of inflammation.[13−16] Upon stimulation, the membrane-associated enzyme NAPE-PLD synthesizes all different FAEs from their corresponding N-acyl phosphatidylethanolamine (NAPE),[9,17,18] a ubiquitous and abundant glycerophospholipid mostly found in tissues and biological fluids that are involved in degenerating processes.[19]

The crystal structure of human NAPE-PLD obtained recently in our laboratory at 2.65 Å of resolution[20] disclosed how the dinuclear zinc active site of the enzyme recognizes NAPE and catalyzes the production of FAEs. Structural and functional analysis unveiled that the secondary bile acid (BA) deoxycholic acid (DCA) binds the protein dimer, in a specific cavity close to the active site (Figure 1). Results showed the interaction between NAPE-PLD and the steroid acid was a stimulus for the enzyme hydrolytic process.[20] This discovery cast an interesting light on NAPE-PLD as a point where FAE signaling and BA physiology converge.[21] However, despite the relevance of this lipidic cross-talk, the chemical determinants of BAs contributing to turn the enzyme on remain unclear.[22]

Here, we have investigated structure−activity correlations and binding kinetics of different natural BAs and identified the steroidal hydroxylation pattern as the key element for enzyme recognition and activation. We have also evaluated the effect of DCA on NAPE-PLD dynamics by neutron scattering (NS), to characterize how the enzyme activation occurs. NS experiments provide quantitative measurements of the thermal mean square atomic fluctuations, and information on global protein

Received: July 21, 2016
Accepted: August 29, 2016
Published: August 29, 2016

DOI: 10.1021/acschembio.6b00624
ACS Chem. Biol. 2016, 11, 2908−2914

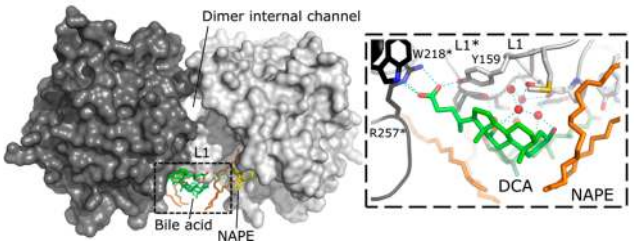

Figure 1. Structure of human NAPE-PLD and bile acid interactions. Surface representation of the NAPE-PLD protein dimer (PDB code: 4qn9). The two subunits (dark gray and light gray) are partly separated by an internal channel having a diameter of ∼9 Å. The subunits interact mainly thought their L1 loops. These loops bind bile acid molecules (carbon atoms in green) and the glycerophospholipidic substrate N-arachydonyl-PE (carbon atoms of the sn-1 and sn-2 fatty acid chain are in orange, while those of the sn-3 in yellow). The parallel orientation of the two monomers suggests that both subunits function concurrently by recruiting NAPE substrates from the membrane. The right panel shows details of the interaction between NAPE-PLD and deoxycholic acid (DCA). The bile acid carboxyl group interacts with residue Y159 of the L1 loop, together with W218 and arginine R257 of the opposite dimer subunit (highlighted by asterisks). The steroid hydroxyls form a network of hydrogen bonds (dotted lines) that involves five L1-bridging water molecules (red spheres). Single-letter abbreviations of amino acids have been used for clarity.

dynamics on a time scale from picoseconds to nanoseconds.[23,24] Results show that, in the presence of DCA, the enzyme limits protein structure fluctuations and enhances its maximum catalytic reaction rate toward the unsatured substrate N-arachydonyl-PE, as determined by lipid chromatography mass spectrometry.

RESULTS AND DISCUSSION

Structure−Activity Relationships of Natural Bile Acids as NAPE-PLD Modulators. To investigate how NAPE-PLD recognizes major human endogenous BAs, we measured their binding affinity and kinetics using surface plasmon resonance (SPR) with fast-step injections.[25] For each compound sensorgram, the values of label-free biomolecular interaction expressed as an association constant, k_a (M^{-1} s^{-1}), dissociation constant, k_d (s^{-1}), and binding constant, $K_D = k_d/k_a$ (μM), are reported in Figure 2A. Interaction kinetics of different BAs showed similar fast association and dissociation rates (Figure 2B), in line with the constitutively exposed binding site on the surface of the protein dimer (Figure 1). The affinities of BAs spanned from ∼20 μM to ∼1 mM, and BAs had similar dissociation constants (from 0.5 s^{-1} to 2.5 s^{-1}). Stronger binders showed values of k_a on the order of $\sim 10^4$ M^{-1} s^{-1}, while weaker binders had values of k_a on the order of $\sim 10^3$ M^{-1} s^{-1}, suggesting the kinetics of association mainly influences the affinity of BAs.

The monohydroxy BA lithocholate (LCA, 3α) showed the highest affinity for NAPE-PLD ($K_D \approx 20$ μM; Figure 2A). The dihydroxy BAs, chenodeoxycholic acid (CDCA, 3α 7α) and deoxycholate acid (DCA, 3α 12α), had a $K_D \approx 25$ μM and ≈ 43 μM, respectively. The addition of a third hydroxyl group to the steroid acid moiety reduced by ∼10-fold the interaction affinity, as the trihydroxy cholic acid (CA, 3α 7α 12α) bound weakly to the enzyme ($K_D \approx 403$ μM; Figure 2A). These results revealed that the enzyme bound preferentially more hydrophobic BAs, and it was sensitive to the presence and position of hydroxyl groups at the steroidal body. The correlation trend between affinities and hydroxyl groups resulted also for natural BAs that were conjugated with glycine and taurine (Figure 2A). For example, glycodeoxycholic acid (GDCA) and taurodeoxycholic acid (TDCA) showed binding affinities that were similar to that observed for DCA, while the affinities of taurocholic acid (TCA) and the synthetic cholic acid-derivative CHAPS were ∼10-fold lower (Figure 2A).

Interestingly, despite a different side chain substitution in position C17 (Figure 2A), the bile acid-analogue fusidic acid (FA) exhibited a $K_D \approx 70$ μM (Figure 2A). The structure of this natural antibiotic[26,27] had two free hydroxyl groups in α-orientation (3α, 11α) that could contribute to the interaction with the enzyme. These observations indicate that the number and orientation of the free hydroxyls drive the interaction between the bound steroid and the protein dimer, possibly involving water molecules located in between (Figure 1).

Comparative dose−response curves in the fluorescence-based activity assay showed that both DCA and CDCA activated NAPE-PLD upon binding, and DCA was slightly more efficient ($EC_{50} \approx 3.2$ mM) at enhancing the activity of the enzyme ($EC_{50} \approx 4.3$ mM; Figure 3A). Their glycine and taurine conjugates also promoted the catalysis of NAPE-PLD, supporting the observation that NAPE-PLD was more sensitive to the hydroxylation in position C12α versus C7α (e.g., GDG, $EC_{50} \approx 2.5$ mM; GCDG, $EC_{50} \approx 3.6$ mM; Figure 3B,C).

As reported above, the monohydroxy BA LCA bound NAPE-PLD (Figure 2). However, LCA was not able alone to solubilize the substrate and activate the membrane enzyme (not shown). We thus evaluated its effect in the presence of DCA at 0.2% (w/v), where the enzyme had maximum activity.[20] Contrary to other examined natural BAs, LCA was shown to inhibit the DCA-induced activation of the enzyme with an $IC_{50} \approx 68$ μM (Figure 3D). Overall, these findings highlighted the crucial role of the hydroxyl groups in determining (i) the BA physicochemical profile, (ii) affinity for NAPE-PLD, and (iii) enzyme activation level. We tried to structurally rationalize these results by X-ray crystallography, but unfortunately, all attempts to crystallize NAPE-PLD in complex with different BAs were unsuccessful.

Deoxycholic Acid Restricts Protein Structure Fluctuations. We next asked whether the interaction between BA and NAPE-PLD (Figure 1) affects protein global flexibility. We performed elastic incoherent neutron scattering (EINS) experiments in the presence of different concentrations of DCA at the high-resolution backscattering spectrometer IN13 of the Institut Laue-Langevin (ILL, Grenoble, France), to spotlight possible protein dynamics transitions occurring in the accessible space-time window (∼2 Å in ∼0.1 ns).[28] The compound DCA was selected for the availability of a three-dimensional description of its complex with the enzyme.

From a first visual inspection of the EINS intensities—summed from the available scattering vector (Q) range ($0.3 < Q < 4.9$ $Å^{-1}$) and plotted as a function of temperature (280, 290, 300, and 307 K)—we observed a significant effect of DCA concentration on the dynamics of protein atoms (Figure 4A). The EINS experiments were carried out in D_2O buffer, at DCA concentrations of 0.00%, 0.05%, 0.15%, 0.50%, and 1.00% (w/v), corresponding to BA/NAPE-PLD ratios of 0.0, 0.5, 1.5, 5.0, and 10.0, respectively. Indeed, in the absence of DCA, the normalized sum of elastic intensities decreased almost linearly with the temperature, and the scattering intensities were almost not affected by the addition of DCA up to a concentration of

DOI: 10.1021/acschembio.6b00624
ACS Chem. Biol. 2016, 11, 2908−2914

A

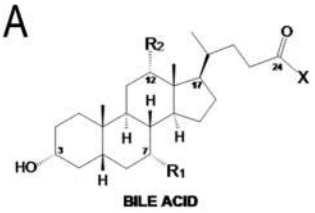

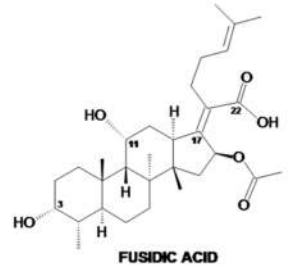

Bile Acid	Structure			Binding kinetics parameters		
	$R1_{(7)}$	$R2_{(12)}$	$X_{(24)}$	k_a (M^{-1} s^{-1})	k_d (s^{-1})	K_D (μM)
Deoxycholic acid (DCA)	H	OH	OH	1.57(3) x 10^4	0.686(2)	43.7(4)
ChenoDCA (CDCA)	OH	H	OH	2.24(1) x 10^4	0.563(1)	25.1(1)
Cholic acid (CA)	OH	OH	OH	6.21(1) x 10^3	2.50(1)	403(2)
Lithocholic acid (LCA)	H	H	OH	2.24(1) x 10^4	0.563(1)	20.3(2)
Glyco-DCA (GDCA)	H	OH	$NHCH_2CO_2H$	1.94(6) x 10^4	1.04(3)	53(3)
Glyco-CDCA (GCDCA)	OH	H	$NHCH_2CO_2H$	1.51(6) x 10^4	0.81(3)	54(3)
Glyco-CA (GCA)	OH	OH	$NHCH_2CO_2H$	3.55(4) x 10^3	3.75(8)	1057(5)
Tauro-DCA (TDCA)	H	OH	$NHCH_2CH_2SO_3H$	2.3(1) x 10^4	1.07(5)	47(1)
Tauro-CA (TCA)	OH	OH	$NHCH_2CH_2SO_3H$	2.22(6) x 10^3	0.981(3)	442(2)
CHAPS	OH	OH	$NH(CH_2)_3N^+(CH_3)_2(CH_2)_3SO_3H$	3.95(9) x 10^3	1.262(2)	319(1)
Fusidic acid (FA)	H	$OH_{(11)}$	$OH_{(22)}$	2.50(2) x 10^4	1.766(3)	70.7(5)

B

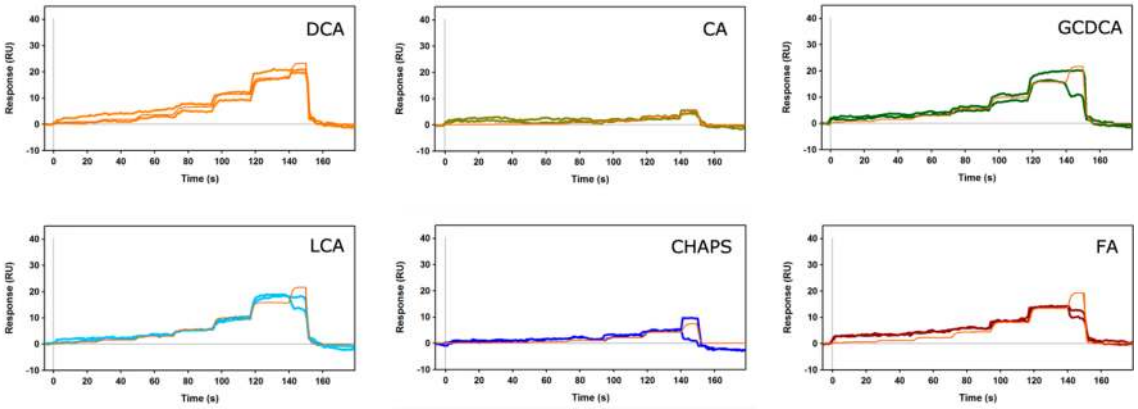

Figure 2. Bile acid recognition by NAPE-PLD. (A) Kinetics parameters of bile acids and compound analogues (CHAPS, Fusidic acid) against NAPE-PLD, determined at 25 °C using surface plasmon resonance. (B) FastStep kinetics response profiles (and their replicates) for selected compounds. The concentration profile of the association phase was created within the biosensor SensiQ Pioneer using a 2-fold dilution series and 100 μM as the highest analyte concentration. Red lines show a global fit to the response data used to extract the binding constants reported in the table (A).

0.15% (w/v). On the contrary, the protein atomic fluctuations were not linear when the concentration of DCA exceeded ∼5 times that of the enzyme (Figure 4B).

We further quantified how much the protein flexibility was affected by the increase of DCA concentration, measuring the temperature dependence of the atomic mean square displacement $\langle u^2 \rangle$ (Å^2; Figure 4B), which was calculated using eq 2 (Methods). The slope of the scan represented the protein dynamics (pseudo)-force constant k (N/m)—eq 3 (Methods)—or "resilience" of the protein, as introduced by Zaccai.[23] The moderate reduction of the k value to the increase of the molar ratio between DCA and protein (Figure 4B) suggested an initially slightly higher protein mobility acquired by NAPE-PLD, possibly due to the presence of the BA detergent molecules in solution. On the other hand, at a higher concentration of DCA (∼10 times that of the enzyme), the system lost flexibility, and the DCA-mediated restriction of protein dynamics fluctuations became evident with the increase of the k value (Figure 4B). Interestingly, the reported crystal structure of NAPE-PLD[20] showed coordinates for 11 molecules of DCA bound to the protein dimer (Figure 1), suggesting how these molecules might contribute to the stiffness of the enzyme (Figure 4C).

Bile Acids Regulate the Biosynthesis of FAEs. To study whether bound BA molecules regulate enzyme substrate specificity, we measured the enzyme kinetic parameters against N-arachidonoyl-PE and N-palmitoyl-PE in the presence of DCA (0.2% w/v; Figure 5). Lipid mass spectrometry electrospray ionization results showed K_m values of ∼9 μM for both substrates, suggesting a similar affinity for NAPE-PLD. These values were consistent with those obtained previously using a radioactivity-based assay (∼3 μM), where the enzymatic reactions were performed in a buffer solution containing the synthetic detergent Triton X-100 (0.1%) for substrate solubilization and enzyme activation.[18]

Despite similar K_m values, in the presence of the cofactor DCA the values of V_{max} were ∼1131 nmol/min/mg protein for N-arachidonoyl-PE and ∼156 nmol/min/mg protein for N-palmitoyl-PE (Figure 5), revealing that the enzyme was not equally active against NAPE with different *N*-acyl groups. Hence, the DCA-complexed NAPE-PLD resulted much faster in hydrolyzing the more unsatured substrate N-arachidonoyl-PE with respect to N-palmitoyl-PE. Indeed, when the specific

DOI: 10.1021/acschembio.6b00624
ACS Chem. Biol. 2016, 11, 2908−2914

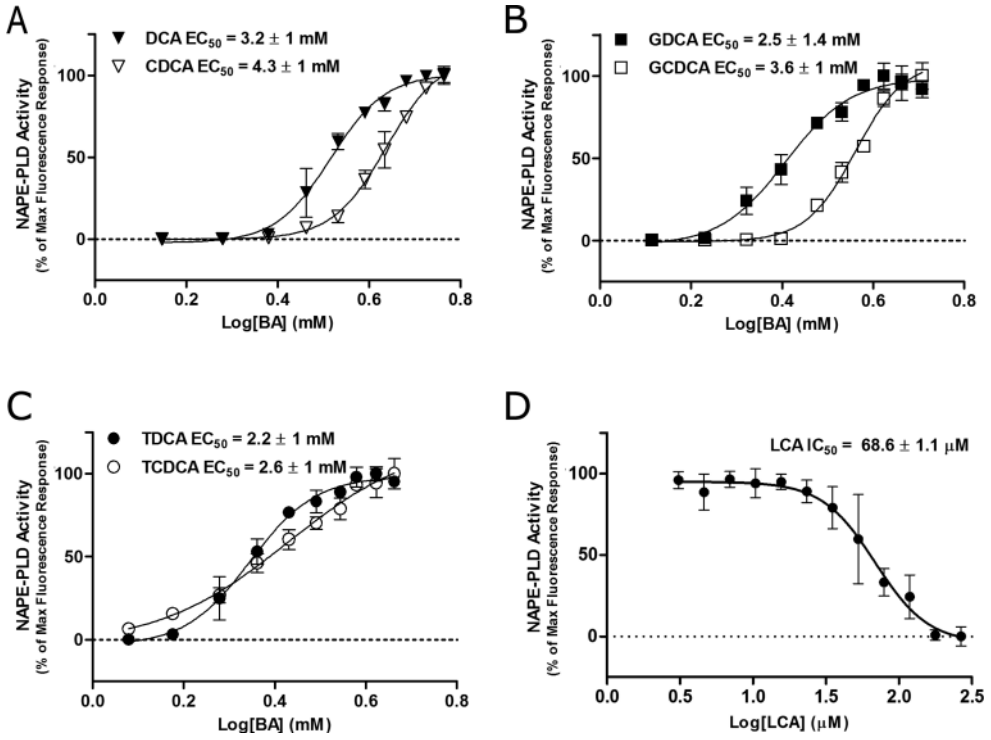

Figure 3. Modulation of NAPE-PLD enzyme activity by different natural bile acids. (A–D) Effect of different bile acids on enzyme activity, expressed as fluorescence spectroscopic changes observed during turn-on/-off assay. All graphs were obtained by fluorescence-based assay following the reaction (at 25 °C for 30 min) between the enzyme (25 nM), preincubated with increasing concentrations of the bile acids, and the substrate PED6. LCA was tested in the presence of DCA (0.2%) to solubilize the substrate (D).

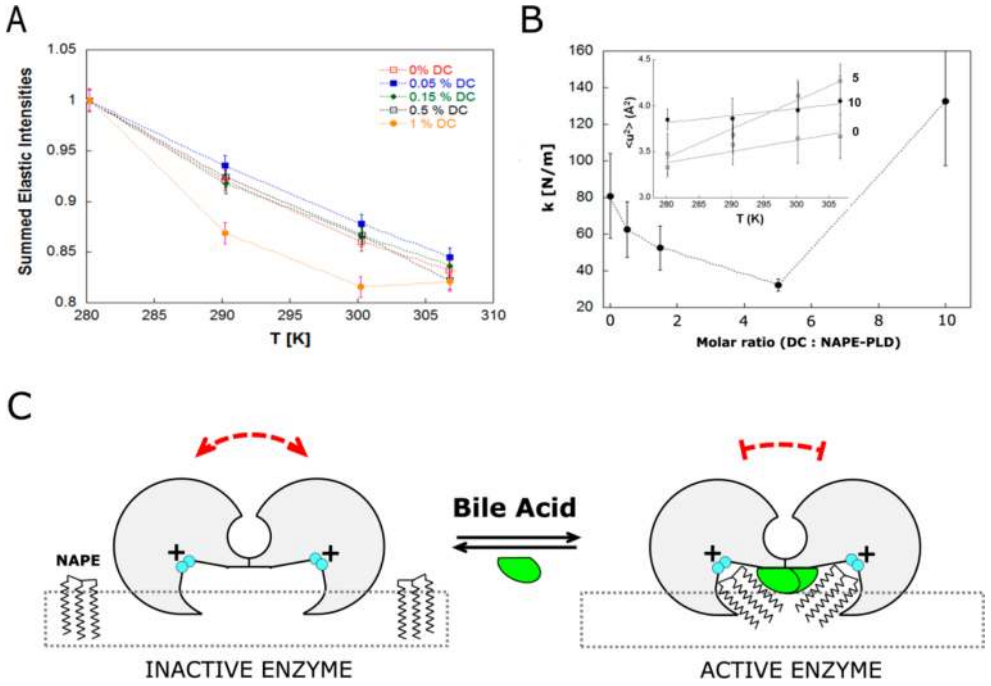

Figure 4. Interaction of bile acids restricting NAPE-PLD structure fluctuations. (A) Elastically scattered intensity binned over the explored range of momentum transfer (Q) as a function of temperature for NAPE-PLD at different concentrations of the bile acid DCA (left panel). (B) Dependence of the force constant k (resilience) upon the molar ratio [DCA : NAPE-PLD]. Inset: temperature dependence of the mean square displacements ($\langle u^2 \rangle$) for the complex between NAPE-PLD and DCA, at molar ratios of 0, 5, and 10. (C) Hypothetical mechanism of bile-acid-mediated restriction of protein dynamics. Functional, structural, and dynamics measurements are consistent with a model where bile acids (green) promote the assembly of inactive NAPE-PLD subunits (gray) into an active dimer, which has reduced dynamics. The resulting lipid–protein complex can recognize the substrate NAPE at the membrane interface (square dots) to promote its hydrolysis. The positively charged binuclear zinc center of the active site is colored in cyan.

DOI: 10.1021/acschembio.6b00624
ACS Chem. Biol. 2016, 11, 2908–2914

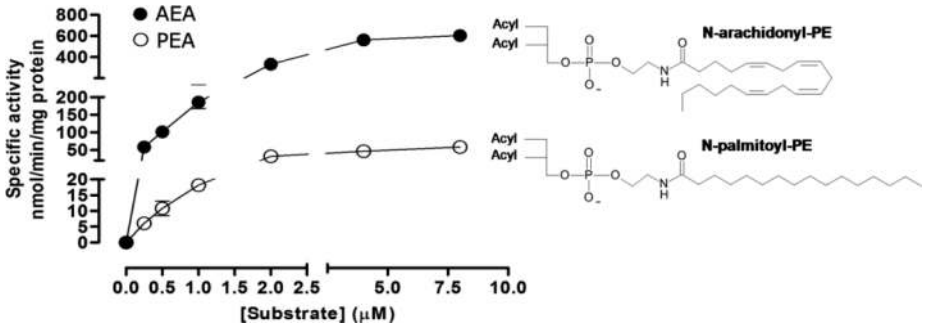

Figure 5. Rate of the bile-acid activated enzyme versus NAPE. Human NAPE-PLDs (0.63 μg of protein) were allowed to react with various concentrations of the substrates N-arachidonoyl-PE and N-palmitoyl-PE in the presence of the cofactor DCA (0.2%, corresponding to the maximum enzyme activation), at 37 °C for 15 min. The graph shows actual data points for the products arachidonylethanolamide (AEA, solid symbols) and palmitoylethanolamide (PEA, open symbols), their best fit line (Prism software). K_m values for the two substrates were 9.6 (±4.2) μM and 9.2 (±1.9) μM, respectively. The maximum velocity (V_{max}) resulted in 1131 (±124.4) nmol/min/mg protein for N-arachidonoyl-PE and 155.8 (±38.36) nmol/min/mg protein for N-palmitoyl-PE. UPLC-MS/MS assays were repeated three times for each substrate.

interaction of BAs for NAPE-PLD had not been discovered yet, the values of V_{max} were reported to be similar (~73 nmol/min/mg and ~98 nmol/min/mg, respectively).[18] Consistent with our results, measurements obtained recently by brain lipidomics analysis showed that all FAEs were significantly reduced in both the "Luquet line" and "Deutsch line" of NAPE-PLD(−/−) knockout mice.[29] However, in the "Luquet line," the magnitude of the effect was stronger for N-arachidonoyl ethanolamine and other unsaturated long N-fatty acid chains (N-docosahexaenoyl ethanolamine and N-linoleoyl ethanolamine), compared with N-oleoyl ethanolamine and N-palmitoyl ethanolamine.[29]

Conclusions. In the present study, we have identified the structural determinants of BAs responsible for recognition and modulation of NAPE-PLD and investigated how this process occurs. Our analyses demonstrate that the enzyme recognizes the cofactors for the number and position of hydroxyl groups at the steroidal body. The hydroxylation pattern of BAs anchors the BA to the L1 loops that interconnect the two protein subunits and contributes to cluster a small number of water molecules at the BA-enzyme interface (Figure 1). Structure[20] and protein dynamics show that when molecules of BA are bound to their allosteric binding sites, the amplitudes of protein thermal motions are restricted, facilitating the active site pocket to accommodate different NAPEs and stimulating the enzyme to promote the catalysis (Figure 4C). Importantly, the complex BA-enzyme enhances the reaction rate with the substrate N-arachidonoyl-PE, suggesting the interaction between NAPE-PLD and BAs, and the stiffening of the enzyme dynamics might favor the selective production of the endocannabinoid anandamide and other unsatured long FAEs. Contrary to DCA, the secondary BA LCA inhibits the enzyme activation in the low micromolar range (~68 μM). We attempted to investigate by X-ray crystallography how LCA might promote this effect, but high concentrations of DCA (>2.0 mM) were indispensable to efficiently solubilize and crystallize the membrane protein, thus preventing LCA binding. However, this observation supports the hypothesis that the ratio between the hydrophobic and cytotoxic LCA[30] and DCA might affect the regulation of FAE biosynthesis. Major free and conjugated dihydroxy BAs function similarly as cofactors to activate NAPE-PLD, providing information that may guide the design of specific BA-based allosteric enzyme modulators.

In vitro, the BA concentration required for a half-maximal response spans from ~2 to ~4 mM. Consequently, dihydroxy BAs bind and activate NAPE-PLD at concentrations that can be found in the gut during food digestion, where the total mean postprandial concentrations of BAs span from ~10 mM in the upper ileum to ~2 mM in the lower ileum.[31] On the contrary, we expect that the trihydroxy bile acid CA might result in being poorly associated with NAPE-PLD, considering that it has a ~10-fold lower binding affinity for the enzyme (this work); the two primary BAs, CDCA and CA, show a similar content in the human BA pool (~40%), and dihydroxy conjugates comprised 76% of the primary BAs in the serum.[32−35] *In vivo* studies are required to assess the physiological meaning of our findings.

METHODS

Protein Expression and Purification. Protein expression and purification were performed as described in ref 20. pMAL c5x vector harboring the gene of *nape-pld* (Δ47) was transformed into *Escherichia coli* RosettagamiB (DE3) pLysS cells (Novagen) to overexpress the encoded recombinant protein with an N-terminus maltose binding protein (MBP) tag and a C-terminus hexahistidine tag. The cells were first grown at 37 °C to an absorbance at 600 nm of 0.7, and protein expression was induced with 250 μM isopropyl-β-D-thiogalactoside (IPTG; Sigma) at 28 °C for 16 h. The cells were then harvested by centrifugation (4500*g*, 20 min, 4 °C), treated with 1 mg mL^{-1} of lysozyme, and frozen at −20 °C.

Cells were then resuspended in ice cold lysis buffer 0.02 M HEPES at pH 7.8, 0.2 M NaCl, and EDTA free protease inhibitor cocktail (Sigma) and lysed by sonication on ice. After removal of the debris by centrifugation (12 000*g*, 1 h, 4 °C), the supernatant was mixed with 5 mL of amilose sepharose resin (New England Biolabs) and incubated on a rotor for 4 h at 4 °C. The MBP-tagged protein was then eluted using lysis buffer without protease inhibitors and digested with recombinant factor Xa protease (Sigma-Aldrich) according to the manufacturer's suggestions.

The protein was finally purified by using Ni-affinity (eluting with 0.02 M HEPES at pH 7.8, 0.2 M NaCl and 500 mM imidazole) and size-exclusion chromatography with a Superdex 16/600 200pg (GE Healthcare) column pre-equilibrated with a buffer of 0.02 M HEPES at pH 7.8 and 0.2 M NaCl in the absence or presence of 0.1% sodium deoxycholate acid (DCA).

Binding Kinetics. Kinetic parameters of the interaction between NAPE-PLD and bile acids were measured by SPR (surface plasmon resonance) using FastStep injections[25] at 25 °C (Biosensor SensíQ Pioneer, ICX Technologies). The protein sample was minimally biotinylated on ice for 3 h using an equimolar concentration of sulfo-NHS-LCA-biotin and passed through a Superdex-200 gel filtration column (buffer 0.02 M HEPES at pH 7.8, 0.2 M NaCl) to remove the excess of free biotin. Streptavidin was immobilized onto a $COOH_5$ sensor chip using a standard amine-coupling method and HBS as a running buffer. This coupling method resulted in a density of ~15 000

DOI: 10.1021/acschembio.6b00624
ACS Chem. Biol. 2016, 11, 2908−2914

RU (resonance units) of neutravidin on all flow cells. Biotinylated NAPE-PLD (Δ47) was then captured to densities of ∼3000 RU. The kinetic profile of BA binding was obtained using 100 μM as the highest concentration and Faststep injections at a flow rate of 30 μL/min. The response data were processed with the QDAT program of the biosensor using a reference surface to correct for any bulk refractive index changes and blank injections for double referencing. The binding profiles were fit globally to a 1:1 interaction model.

Neutron Scattering. Incoherent neutron scattering of protein samples is dominated by hydrogen atoms,[23] because hydrogen comprises approximately 50% of all protein atoms, and the incoherent scattering cross sections of hydrogen (80.27 barn) is significantly larger than that of other atoms in biological macromolecules (nitrogen 0.5 barn, carbon and oxygen 0.001 barn). Hydrogen atoms are homogeneously distributed in biological macromolecules; thus neutron scattering can probe average molecular dynamics. In order to enhance the scattering contribution of NAPE-PLD atoms and neglect that of the buffer, the purified protein was concentrated and resuspended five times against a 100× volume of D_2O (deuterium 2.08 barn).

Temperature-dependent EINS scans were performed on the thermal neutron high resolution backscattering spectrometers IN13 of the Institut Laue-Langevin (ILL), Grenoble, France. With a nearly Q-independent energy resolution of δE = 8 μeV (full width at half-maximum) and an accessible momentum transfer range of 0.2 < Q < 4.9 $Å^{-1}$, IN13 allows the investigation of molecular motions on a time scale up to 100 ps and with an amplitude from 1.3 Å to ∼31 Å. Elastic neutron scattering spectra of NAPE-PLD (100 mg mL^{-1}) were collected in the temperature range 280−310 K, with ∼3 h of acquisition time per point to optimize the signal-to-noise ratio.

The program LAMP[36] was used for data reduction, consisting of removal of the empty cell contribution and normalization with respect to a vanadium scan (a totally incoherent sample) to compensate for differences in detector efficiency and geometry. In order to avoid corrections from multiple scattering events, cell thickness and geometry were properly chosen to minimize neutron absorption from the sample. A typical transmission of ∼95% was guaranteed using a standard flat aluminum sample holder with a thickness of 0.4 mm.

EINS Data Analysis. The scattered elastic incoherent intensity can be described in a Gaussian approximation by the dynamic structure factor at zero energy exchange.[28,37]

$$S_{el}(Q, \omega = 0 \pm \Delta E) \approx S_0 \exp\left(-\frac{1}{6}\langle u^2\rangle Q^2\right) \quad (1)$$

where ΔE is instrumental energy resolution, related to the time window through Heisenberg's uncertainty principle, and $\langle u^2\rangle$ is the average time-dependent atomic mean square displacement in the limit defined by ΔE.[38]

Similarly to the Guinier approximation in small angle scattering, the Q range of validity for the Gaussian approximation depends on the geometry of the motion and could go as far as $\langle u^2\rangle\ Q^2 \approx 2$.[39] For each temperature the $\langle u^2\rangle$ can be obtained by the slope of the semilogarithmic plot of the incoherent scattering function through

$$\langle u^2\rangle \approx -6\frac{d\ \mathrm{In}\ S_{el}(Q, \omega = 0 \pm \Delta E)}{dQ^2} \quad (2)$$

An effective average force constant for sample dynamics, $\langle k\rangle$, can be calculated from the slope of $\langle u^2\rangle$ as a function of temperature, by applying a quasi-harmonic approximation:[23]

$$\langle k\rangle = \frac{0.00276}{d\langle u^2\rangle/dT} \quad (3)$$

Enzyme Activity Assays. The activity of NAPE-PLD in the presence of different BAs was measured by fluorescence assay as described previously.[20] Briefly, the enzyme was diluted to a final concentration of 25 nM in assay buffer (50 mM Tris-HCl, pH 8), preincubated for 1 h at RT with varying concentrations of bile acids (0−5 mM). The substrate PED6 [N-((6-(2,4-dinitrophenyl)amino)-hexanoyl)-2-(4,4-difluoro-5,7-dimethyl-4-bora-3a,4a-diaza-s-indacene-3-pentanoyl)-1-hexadecanoyl-*sn*-glycero-3-phosphoethanolamine, triethylammonium salt] in 2.5% DMSO/ethyl acetate (1:4 v/v) was added to a final concentration of 10 μM in the reaction buffer (1% DMSO/ethyl acetate mixture) and the fluorescence measured after 30 min of incubation in the dark at 25 °C, using an emission filter at 485 nm and excitation filter at 535 nm. The effect on activity of LCA was measured in the presence of 0.2% w/v DCA in the reaction buffer to solubilize the substrate and activate the enzyme. Plates were finally incubated for 30 min at 25 °C in the dark. Reaction fluorescence was measured using the EnVision 2104 Multilabel Plate Reader and results analyzed by Prism software.

The effect of DCA on enzyme kinetics was measured in multiple reaction monitoring by ultraperformance liquid chromatography tandem mass spectrometry (UPLC-MS/MS). The protein (630 ng) was incubated with different substrate concentrations, N-arachidonoyl-PE or N-palmitoyl-PE, in [0.3 mL of 0.05 M Tris-HCl buffer at pH 7.4, 0.2% w/v DCA], for 15 min at 37 °C. Reactions were stopped by ther addition of cold acetonitrile containing either PEA-d4 or AEA-d4 as an internal standard, assuming that a steady state was reached (Michaelis Menten condition). After centrifugation (3000*g* at 4 °C for 20 min), the organic layers were collected and used for the UPLC-MS/MS acquisition. LC-MS/MS analyses were carried out on an Acquity UPLC system coupled with a Xevo TQ-MS triple quadrupole mass spectrometer (Waters Inc. Milford, MA, USA). Chromatographic separation was achieved using a BEH C18 column and a flow rate elution of 0.5 mL/min. Analytes were quantified by multiple reaction monitoring (MRM) in the positive ESI mode. Data were acquired by MassLynx software and quantified by TargetLynx software. Calibration curves were obtained by plotting the analyte to IS peak areas ratio versus the corresponding analyte concentration using weighted $(1/x)$ least-squares regression analysis. Each experiment was run in triplicate. Prism software was used to fit the velocity/concentration profiles and determine the Michaelis Menten kinetic parameters (V_{max} and K_m) for the products arachidonylethanolamide and palmitoylethanolamide.

AUTHOR INFORMATION

Corresponding Author

*E-mail: gianpiero.garau@iit.it.

Present Address

#IRBM Science Park, Pomezia, Italy.

Author Contributions

E.M., S.P., and F.N. performed and analyzed neutron scattering studies. P.M. designed and performed SPR assays. B.C., P.M., and E.R. performed fluorescence and LC-MS assays. S.M. analyzed bile acid purity. G.G. directed the project, designed experiments, analyzed and interpreted the results, and wrote the manuscript, together with A.G. and D.P.

Notes

The authors declare no competing financial interest.

ACKNOWLEDGMENTS

The financial support of Marie Curie Action IRG (FP7-PEOPLE-2010-RG, contract no PIRG07-GA-2010-268385 to P.M.) and the National Institute on Drug Abuse (grants DK073955 and DA012413 to D.P.) is gratefully acknowledged. We thank A. Armirotti, L. Bono, and M. Pini for assistance with systems of mass spectrometry and liquid handling.

REFERENCES

(1) Wymann, M. P., and Schneiter, R. (2008) Lipid signalling in disease. *Nat. Rev. Mol. Cell Biol. 9*, 162−176.

(2) Piomelli, D. (2003) The molecular logic of endocannabinoid signalling. *Nat. Rev. Neurosci. 4*, 873−884.

(3) Williams, C. M., and Kirkham, T. C. (1999) Anandamide induces overeating: mediation by central cannabinoid (CB1) receptors. *Psychopharmacology (Berl) 143*, 315−317.

DOI: 10.1021/acschembio.6b00624
ACS Chem. Biol. 2016, 11, 2908−2914

(4) Zygmunt, P. M., Petersson, J., Andersson, D. A., Chuang, H., Sorgard, M., Di Marzo, V., Julius, D., and Hogestatt, E. D. (1999) Vanilloid receptors on sensory nerves mediate the vasodilator action of anandamide. *Nature 400*, 452−457.
(5) Di Marzo, V., Goparaju, S. K., Wang, L., Liu, J., Batkai, S., Jarai, Z., Fezza, F., Miura, G. I., Palmiter, R. D., Sugiura, T., and Kunos, G. (2001) Leptin-regulated endocannabinoids are involved in maintaining food intake. *Nature 410*, 822−825.
(6) Hansen, H. S. (2014) Role of anorectic N-acylethanolamines in intestinal physiology and satiety control with respect to dietary fat. *Pharmacol. Res. 86*, 18−25.
(7) Osei-Hyiaman, D., DePetrillo, M., Pacher, P., Liu, J., Radaeva, S., Batkai, S., Harvey-White, J., Mackie, K., Offertaler, L., Wang, L., and Kunos, G. (2005) Endocannabinoid activation at hepatic CB1 receptors stimulates fatty acid synthesis and contributes to diet-induced obesity. *J. Clin. Invest. 115*, 1298−1305.
(8) Ledent, C., Valverde, O., Cossu, G., Petitet, F., Aubert, J. F., Beslot, F., Bohme, G. A., Imperato, A., Pedrazzini, T., Roques, B. P., Vassart, G., Fratta, W., and Parmentier, M. (1999) Unresponsiveness to cannabinoids and reduced addictive effects of opiates in CB1 receptor knockout mice. *Science 283*, 401−404.
(9) Berghuis, P., Rajnicek, A. M., Morozov, Y. M., Ross, R. A., Mulder, J., Urban, G. M., Monory, K., Marsicano, G., Matteoli, M., Canty, A., Irving, A. J., Katona, I., Yanagawa, Y., Rakic, P., Lutz, B., Mackie, K., and Harkany, T. (2007) Hardwiring the brain: endocannabinoids shape neuronal connectivity. *Science 316*, 1212−1216.
(10) Fu, J., Gaetani, S., Oveisi, F., Lo Verme, J., Serrano, A., Rodriguez De Fonseca, F., Rosengarth, A., Luecke, H., Di Giacomo, B., Tarzia, G., and Piomelli, D. (2003) Oleylethanolamide regulates feeding and body weight through activation of the nuclear receptor PPAR-alpha. *Nature 425*, 90−93.
(11) Schwartz, G. J., Fu, J., Astarita, G., Li, X., Gaetani, S., Campolongo, P., Cuomo, V., and Piomelli, D. (2008) The lipid messenger OEA links dietary fat intake to satiety. *Cell Metab. 8*, 281−288.
(12) Folick, A., Oakley, H. D., Yu, Y., Armstrong, E. H., Kumari, M., Sanor, L., Moore, D. D., Ortlund, E. A., Zechner, R., and Wang, M. C. (2015) Aging. Lysosomal signaling molecules regulate longevity in Caenorhabditis elegans. *Science 347*, 83−86.
(13) Lo Verme, J., Fu, J., Astarita, G., La Rana, G., Russo, R., Calignano, A., and Piomelli, D. (2005) The nuclear receptor peroxisome proliferator-activated receptor-alpha mediates the anti-inflammatory actions of palmitoylethanolamide. *Mol. Pharmacol. 67*, 15−19.
(14) Solorzano, C., Zhu, C., Battista, N., Astarita, G., Lodola, A., Rivara, S., Mor, M., Russo, R., Maccarrone, M., Antonietti, F., Duranti, A., Tontini, A., Cuzzocrea, S., Tarzia, G., and Piomelli, D. (2009) Selective N-acylethanolamine-hydrolyzing acid amidase inhibition reveals a key role for endogenous palmitoylethanolamide in inflammation. *Proc. Natl. Acad. Sci. U. S. A. 106*, 20966−20971.
(15) Zhu, C., Solorzano, C., Sahar, S., Realini, N., Fung, E., Sassone-Corsi, P., and Piomelli, D. (2011) Proinflammatory stimuli control N-acylphosphatidylethanolamine-specific phospholipase D expression in macrophages. *Mol. Pharmacol. 79*, 786−792.
(16) Alhouayek, M., and Muccioli, G. G. (2014) Harnessing the anti-inflammatory potential of palmitoylethanolamide. *Drug Discovery Today 19*, 1632−1639.
(17) Di Marzo, V., Fontana, A., Cadas, H., Schinelli, S., Cimino, G., Schwartz, J. C., and Piomelli, D. (1994) Formation and inactivation of endogenous cannabinoid anandamide in central neurons. *Nature 372*, 686−691.
(18) Okamoto, Y., Morishita, J., Tsuboi, K., Tonai, T., and Ueda, N. (2004) Molecular characterization of a phospholipase D generating anandamide and its congeners. *J. Biol. Chem. 279*, 5298−5305.
(19) Schmid, H. H. (2000) Pathways and mechanisms of N-acylethanolamine biosynthesis: can anandamide be generated selectively? *Chem. Phys. Lipids 108*, 71−87.
(20) Magotti, P., Bauer, I., Igarashi, M., Babagoli, M., Marotta, R., Piomelli, D., and Garau, G. (2015) Structure of human N-acylphosphatidylethanolamine-hydrolyzing phospholipase D: regulation of fatty acid ethanolamide biosynthesis by bile acids. *Structure 23*, 598−604.
(21) Kostic, M. (2015) Bile Acids, Chemical Libraries, Ebola Virus, and Bacterial Uracil. *Chem. Biol. 22*, 427−428.
(22) Zorn, J. A., and Wells, J. A. (2010) Turning enzymes ON with small molecules. *Nat. Chem. Biol. 6*, 179−188.
(23) Zaccai, G. (2000) How soft is a protein? A protein dynamics force constant measured by neutron scattering. *Science 288*, 1604−1607.
(24) Frauenfelder, H., and Mezei, F. (2010) Neutron scattering and protein dynamics. *Acta Crystallogr., Sect. D: Biol. Crystallogr. 66*, 1229−1231.
(25) Rich, R. L., Quinn, J. G., Morton, T., Stepp, J. D., and Myszka, D. G. (2010) Biosensor-based fragment screening using FastStep injections. *Anal. Biochem. 407*, 270−277.
(26) Godtfredsen, W. O., Jahnsen, S., Lorck, H., Roholt, K., and Tybring, L. (1962) Fusidic acid: a new antibiotic. *Nature 193*, 987.
(27) Fernandes, P., and Pereira, D. (2011) Efforts to support the development of fusidic acid in the United States. *Clin. Infect. Dis. 52* (Suppl 7), S542−S546.
(28) Zaccai, G. (2011) Neutron scattering perspectives for protein dynamics. *J. Non-Cryst. Solids 357*, 615−621.
(29) Leishman, E., Mackie, K., Luquet, S., and Bradshaw, H. B. (2016) Lipidomics profile of a NAPE-PLD KO mouse provides evidence of a broader role of this enzyme in lipid metabolism in the brain. *Biochim. Biophys. Acta, Mol. Cell Biol. Lipids 1861*, 491−500.
(30) Hofmann, A. F. (2004) Detoxification of lithocholic acid, a toxic bile acid: relevance to drug hepatotoxicity. *Drug Metab. Rev. 36*, 703−722.
(31) Northfield, T. C., and McColl, I. (1973) Postprandial concentrations of free and conjugated bile acids down the length of the normal human small intestine. *Gut 14*, 513−518.
(32) de Aguiar Vallim, T. Q., Tarling, E. J., and Edwards, P. A. (2013) Pleiotropic roles of bile acids in metabolism. *Cell Metab. 17*, 657−669.
(33) Ahlberg, J., Angelin, B., Bjorkhem, I., and Einarsson, K. (1977) Individual bile acids in portal venous and systemic blood serum of fasting man. *Gastroenterology 73*, 1377−1382.
(34) Hofmann, A. F. (2011) Enterohepatic circulation of bile acids. *Comprehensive Physiology*, John Wiley & Sons, Inc., Hoboken, NJ, DOI: 10.1002/cphy.cp060329.
(35) Angelin, B., Björkhem, I., Einarsson, K., and Ewerth, S. (1982) Hepatic Uptake of Bile Acids in Man: Fasting and postprandial concentrations of individual bile acids in portal venus and systemic blood serum. *J. Clin. Invest. 70*, 724−731.
(36) Richard, D., Ferrand, M., and Kearley, G. (1996) Analysis and visualisation of neutron-scattering data. *J. Neutron Res. 4*, 33−39.
(37) Rahman, A., Singwi, K., and Sjölander, A. (1962) Theory of slow neutron scattering by liquids. *Phys. Rev. 126*, 986.
(38) Vural, D., Hong, L., Smith, J. C., and Glyde, H. R. (2015) Motional displacements in proteins: The origin of wave-vector-dependent values. *Phys. Rev. E 91*, 052705.
(39) Réat, V., Zaccai, G., Ferrand, M., and Pfister, C. (1997) Functional dynamics in purple membrane. *Biol. Macromol. Dyn.*, 117−122.

DOI: 10.1021/acschembio.6b00624
ACS Chem. Biol. 2016, 11, 2908−2914